

Plasma Discharges in Atmospheric Pressure Oxygen for Boundary Layer Separation Control

Gabriel I. Font*
US Air Force Academy, CO, 80840

W. Lowell Morgan
Kinema Research, L.L.C., Monument, CO 80132

Recent studies have shown atmospheric plasma discharges to be an effective means of reattachment of separated boundary layers on airfoils. The plasma acts to impart momentum deep in the boundary layer forestalling separation. Previous plasma simulations in pure nitrogen have shown the temporal behavior of the plasma and clarified the force production mechanism. The present study extends the computations to discharges with oxygen. A particle-in-cell and Monte-Carlo (PIC-DSMC) method is used to numerically explore the nature of the interaction of the negative and positive ions with the fluctuating electric field. The presence of oxygen and, more importantly, the negative oxygen ions generated in the plasma, modify the force production mechanism by providing a new path for momentum addition to the air. Results show that the presence of negative oxygen ions diminishes the net force. The ionization energies for oxygen, however, are lower than nitrogen leading to greater levels of ionization and, consequently, more net force production than discharges in pure nitrogen. Comparisons with experiments are presented to support the findings.

I. Introduction

Recent studies have demonstrated the capability of plasma discharges to promote boundary layer attachment on airfoils at a high angle-of-attack.¹⁻⁵ The plasma discharges accomplish this by supplying additional momentum to the boundary layer^{4,6} and are effective at atmospheric pressures. The plasma discharge is created by a small device called a plasma actuator, shown in Fig. 1. It consists of two electrodes separated by a dielectric. The upper electrode is exposed to the free stream flow while the lower electrode is placed underneath the dielectric. The two electrodes are displaced horizontally from each other. An alternating voltage of 1-10 kV is applied to the electrodes at 1-10 kHz which causes the formation of a plasma in the vicinity of the electrodes. The device is typically mounted flush on the surface of an airfoil.

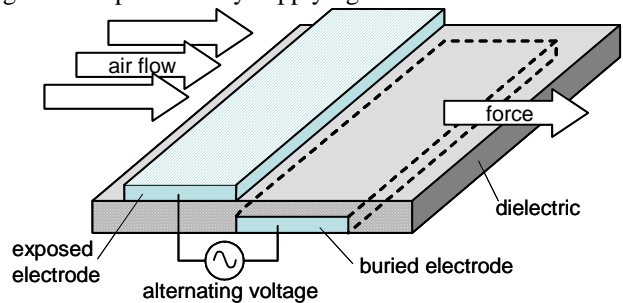


Figure 1. Plasma actuator configuration.

Current studies have focused on exploring the effects of frequency, wave form, Reynolds number, and geometry on the force production, drag reduction, and nature of the plasma actuator.^{4,7-10} In a previous numerical study,¹¹ the force production mechanism of the plasma discharge in pure Nitrogen was investigated. Simulations suggested that the plasma is pulling the N_2 against the prevailing flow during the first half of the bias cycle and pushing during the second half. A net force arises, at least in part, because the plasma density and, therefore, the force production are greater during the second half of the bias cycle. This pulling-pushing effect of the plasma actuator was later measured in an experimental study.¹² The same study also showed significant differences between the force

* Professor, Department of Physics, AIAA Member, Email: Gabriel.font@usafa.af.mil

production levels in pure nitrogen and in air. A reason for this could be the presence of negative ions generated in a plasma which contains oxygen. In order to investigate the differences in the force production mechanisms between nitrogen and air, the present study simulates a plasma actuator in pure oxygen. The comparison between pure oxygen and pure nitrogen discharges is used to shed light on air discharges. Section II details the computational model. Computational results and comparisons to experiments are presented in section III. The majority of the results shown will be for an oxygen discharge since the nitrogen discharges were presented previously in ref. 11.

II. Computational Model

Simulation of the plasma was accomplished using a Particle-In-Cell Direct-Simulation-Monte-Carlo (PIC-DSMC) method. The details of this method have been documented in previous publications.¹³⁻¹⁷ In the PIC method, each computational particle represents from thousands to millions of charged particles of a single species (ion or electron). At each time step, the particle charge is weighted onto a computational grid. Using the charge distribution, Poisson's equation is solved for the electric potential on the grid using an alternating-direction-implicit (ADI) iterative scheme. The local electric fields are calculated from the potential distribution and are weighted back to the positions of the particles. These are, then, used to calculate the forces and accelerations of the charged particles. A leap-frog¹³ method is used calculate the velocities and positions of the particles at the new time step. This sequence is repeated for each time step which allows the plasma to evolve. The present simulation treats both ions and electrons as computational particles.

The computation follows only the charged species. Neutral species are treated as a background gas. As the electrons and ions travel through the flow field, they collide with the ambient nitrogen or oxygen molecules. If they have gained sufficient energy, they may cause ionization, dissociation, and/or meta-stable excitation. The code handles collisions using a Direct-Simulation-Monte-Carlo^{14,15} (DSMC) method. The probability of each particle undergoing a collision during each time step is evaluated using a no-time-counter method.¹⁴ Any chemistry which may take place is computed and the resultant species are added or subtracted to the computation particle list. Any resultant neutral species is added to or subtracted from the background gas. Since the discharge only lasts 10s of nanoseconds, the neutrals do not have sufficient time to move any significant distance. For this reason, neutral species motion is not modeled.

Simulations are initially conducted in pure nitrogen. The chemistry has been updated from ref. 11 and is presented in Table 1. The reactions include momentum transfer, molecular ionization, excitation, dissociation, dissociative recombination, and secondary electron emission. The primary ion is N_4^+ because, at atmospheric pressures, the N_2^+ is converted to N_4^+ (via $N_2^+ + N_2 \rightarrow N_4^+$) at a rate that is as great as the original ionization. For each of these reactions, the collision cross-sections in ref. 18-21 were used to calculate the reaction probabilities. The meta-stable excitation

Table 1. Nitrogen Chemical Reactions

| | | | | | | | |
|---------|-----|-------------|---------------|---------|-----|---------|--|
| e | $+$ | N_2 | \rightarrow | N_2 | $+$ | e | momentum transfer |
| e | $+$ | $2N_2$ | \rightarrow | N_4^+ | $+$ | $2e$ | ionization ($N_2 + N_2^+ \rightarrow N_4^+$) |
| e | $+$ | N_2 | \rightarrow | N_2^* | $+$ | e | meta-stable excitation |
| e | $+$ | N_2 | \rightarrow | $2N$ | $+$ | e | dissociation |
| e | $+$ | N_4^+ | \rightarrow | $2N_2$ | | | dissociative recombination (glow) |
| N_4^+ | $+$ | N_2 | \rightarrow | N_4^+ | $+$ | N_2 | momentum transfer |
| N_4^+ | $+$ | Cu_{surf} | \rightarrow | $2N_2$ | $+$ | $0.03e$ | secondary electron emission |

reaction is a combination of several excitation reactions. The composite cross section is plotted in Fig. 2. The cross-sections for each of the individual excitation reactions were added together and the energy loss to the impacting electrons was computed through out the first 20eV using a weighted average.

Plasma actuators are typically operated in air. The oxygen in the air could significantly alter the discharge due to the presence of negative (O^-) ions. The negative ions add momentum in the opposite direction to the positive ions and oxygen has different recombination, dissociation, and excitation behavior. In order to explore the force production differences between nitrogen and oxygen, computations were also carried out in pure oxygen. This should approximate the air behavior because the plasma in air is thought to be dominated by the oxygen due to its lower ionization energies (12.06 vs 15.6 eV). True air chemistry ($O_2 + N_2$) will be treated in future investigations. The chemical reactions for pure oxygen included in the computations are shown in Table 2.

The chemical reaction set used in the oxygen computations is shown in Table 2. It is similar to the nitrogen set with the addition of a creation reaction (dissociative attachment) and a momentum transfer reaction for the negative oxygen ions. The primary positive ion is O_4^+ because, as with nitrogen, at atmospheric pressure, O_2^+ is converted to O_4^+ as fast as it is created (through $O_2^+ + O_2 \rightarrow O_4^+$). The collision cross sections for oxygen reactions were taken from ref. 19-22.

The computational geometry is shown in Fig. 3. It consists of two electrodes separated by a dielectric. The upper electrode is 0.5 mm thick and protrudes only 0.25 mm into the computational domain. A larger exposed electrode was found unnecessary because previous computations showed that the plasma does not extend significantly beyond of the edge of the electrode. The buried electrode is 1.25 mm long and is a boundary condition below the dielectric. The dielectric is 0.5 mm thick. The computational domain is 1.5 mm high by 2.0 mm long by 0.1 mm wide.

The grid is 165 x 320 cells. In the plasma region, the cells are 6.25×10^{-6} m square (height and length) by 0.1 mm wide. Only every fourth cell in the plasma region is shown in the figure for clarity. The electrode and dielectric thicknesses are chosen to be representative of the experimental setups currently under investigation. The length of the buried electrode was shortened to decrease the computational work load. The computational domain is one cell wide with reflective boundary conditions on either side. Therefore, although all particle motions and collisions are calculated in 3 dimensions, the simulation is effectively only 2 dimensional. Because the experimental electrodes are long and slender, however, the plasma is 2 dimensional to a good approximation.

Particle boundary conditions were as follows: Particles exiting the computational domain were deleted from the computation. Particles striking the exposed electrode would be neutralized and, therefore, were also deleted from the simulation. Particles striking the dielectric were held at the dielectric boundary and their velocity was set to zero. In the actual plasma, an electron or an ion may bury itself into the dielectric due to the impact momentum. This may affect the speed at which the particles leave the dielectric when the electric field reverses since some energy has to be expended to extract them from the surface. It would also affect the timing of their departure since the electric field has to rise above some threshold for extraction. No attempt to model this has yet been made in the current simulation.

Electrical boundary conditions were as follows: The potential gradient was set to zero along the plasma boundaries. The potential was computed by solving the Poisson's equation throughout the domain, including the

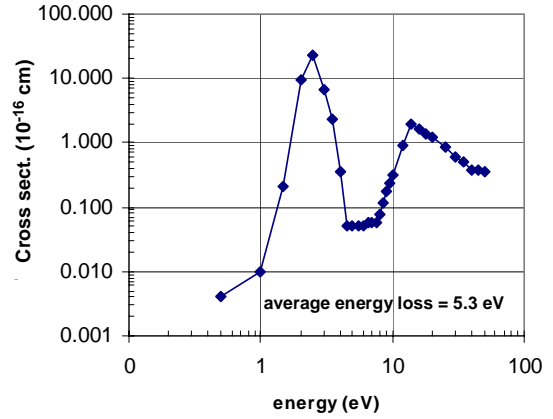


Figure 2. Nitrogen excitation cross section.

Table 2. Oxygen Chemical Reactions

| | | |
|---------------------|----------------------------|--|
| $e + O_2$ | $\rightarrow O_2 + e$ | momentum transfer |
| $e + 2O_2$ | $\rightarrow O_4^+ + 2e$ | ionization ($O_2 + O_2^+ \rightarrow O_4^+$) |
| $e + O_2$ | $\rightarrow O^- + O$ | dissociative attachment |
| $e + O_2$ | $\rightarrow O_2^* + e$ | meta-stable excitation |
| $e + O_2$ | $\rightarrow 2O + e$ | dissociation |
| $e + O_4^+$ | $\rightarrow 2O_2$ | dissociative recombination (glow) |
| $O_4^+ + O_2$ | $\rightarrow O_4^+ + O_2$ | momentum transfer |
| $O^- + O_2$ | $\rightarrow O^- + O_2$ | momentum transfer |
| $O_4^+ + Cu_{surf}$ | $\rightarrow 2O_2 + 0.03e$ | secondary electron emission |

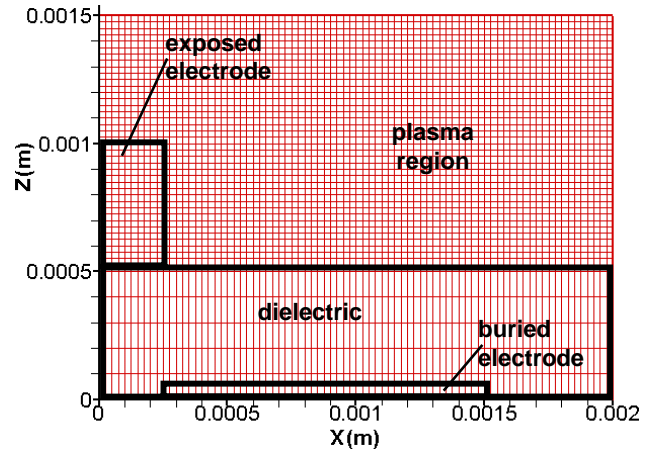


Figure 3. Computational geometry.

dielectric. The dielectric constant is currently set to 3.5. During the simulations, the buried electrode was held at zero Volts, while the exposed electrode was held at either positive or the negative peak voltage. A time varying potential was not attempted since the electron avalanche spans less than 20×10^{-9} sec and the collision frequency with the neutrals forces a time step of about 1×10^{-13} sec. Therefore, capturing even a single bias cycle is prohibitively expensive. Instead, the potential of the exposed electrode was set to the negative peak voltage, for example -5200V and the discharge was computed until it extinguished. This was followed by setting the potential to positive peak voltage and, again, computing the discharge until it extinguishes. Therefore, the simulation utilizes a square wave input to the electrodes. Different grid densities were tried for the simulation. The cell size in the plasma region was reduced from 2.5×10^{-5} m to 0.4×10^{-5} m until the force began to converge. Further reductions were not made due to computational constraints.

The simulations were started by seeding the flow with a small number of electrons. Trials were conducted where the number of seed electrons was reduced until the discharge became independent of the size of the seed. This is a standard technique in this type of simulation.^{16,17} The seed electrons are placed near the upper corner of the exposed electrode where secondary electron or field effect emission is expected. The plasma discharge then evolves self-consistently as the electrons accelerate in the electric field and cause further ionization, dissociation, etc.

III. Computational Results

Simulations were conducted of a 2-dimensional slice of a plasma actuator discharge at atmospheric pressure and density with a square wave input of amplitude ranging from 5000 to 5500 V. The bias frequency is not specified but is low enough to allow the discharge to extinguish before the electrodes reverse polarity. In the present simulation, this results in an effective frequency in the 1-10 mega-Hertz range. Simulations were conducted in pure nitrogen and in pure oxygen separately.

The electric potential contours and the electric field magnitude and vectors are shown in Fig. 4 at a time before the start of the discharge. The exposed electrode is set to 5200 V and the buried electrode is grounded (0 V). The effect of the dielectric is to bring the ground (0V) plane closer to the exposed electrode and increase the effective electric field. The average electric field in the vicinity of the exposed electrode is on the order of 10^7 V/m and points generally toward the exposed electrode. The discontinuity in the potential contour slope is due to the difference in the dielectric constant between the air and the insulating Kapton layer.

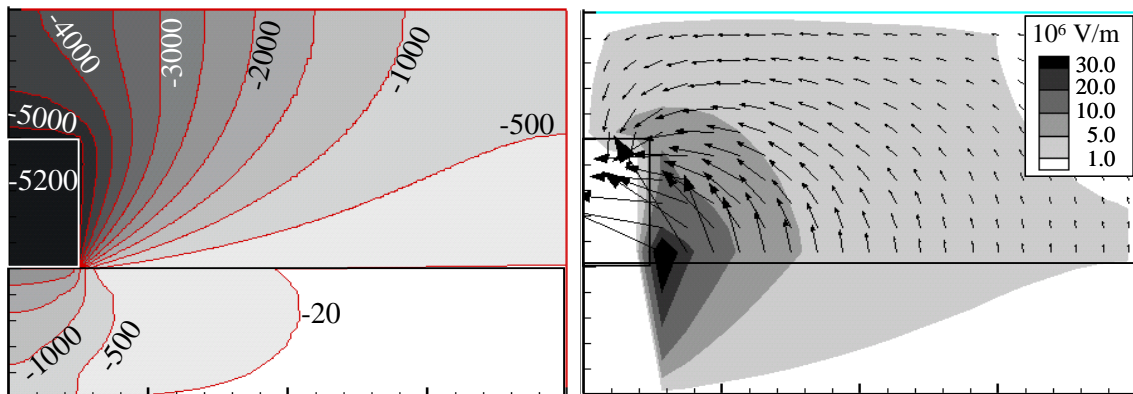


Figure 4. Potential distribution (Volts), electric field magnitude (V/m), and electric field vectors before forward discharge for oxygen, Bias = 5200V.

A. Plasma Discharge

The plasma discharge begins when the exposed electrode is biased negatively. This allows electrons generated through field effect emission to accelerate away from the exposed electrode and gain energy. The part of the discharge where electrons are pushed away from the exposed electrode will be referred to as the ‘forward’ discharge. The beginning of the plasma discharge in oxygen is illustrated in Fig. 5, which shows the charged

particle density during the first 3 nsec. The electrons accelerate along the electric field and, when sufficient energy is gained, cause ionization through collisions with the neutral molecules. The head of the avalanche is predominantly composed of electrons, while the tail of the streamer is dominated by ions. This occurs because the collision cross-section of the ions and electrons with the neutrals are very different, as shown in Fig. 6. Simulations show that the ions typically have a temperature of 0.05 eV while the electrons have a temperature of 0.5-1.0 eV. The collision probability for the ions, determined with the cross-section, therefore, is about 100 times greater for the ions than for the electrons. The result is that the electrons suffer fewer collisions and, therefore, stream through the neutrals while the ions, a great many more collisions, are effectively kept from moving very far. Note: charge density contours inside the dielectric are a graphing artifact. In the simulation, particles are stopped at the surface of the dielectric and not allowed to move into the dielectric.

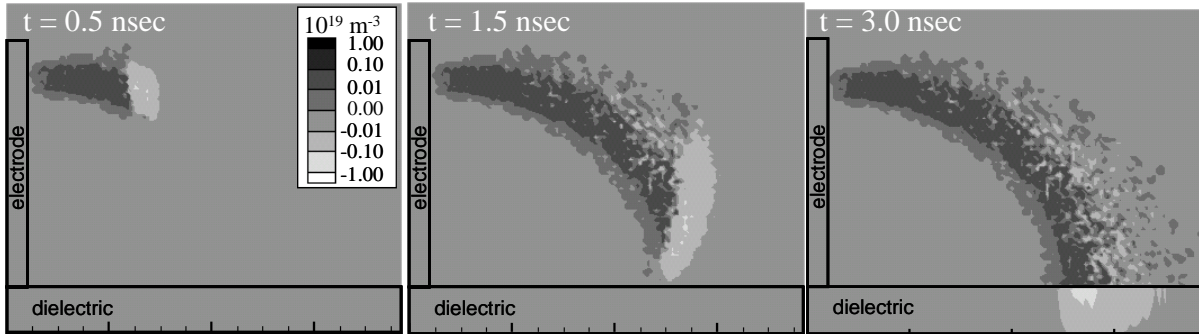


Figure 5. Charge number density throughout the beginning of the forward discharge; Bias=5200V.

Figure 7 shows the electron, positive ion, and negative ion density at $t = 1.0$ nsec. Most of the electrons are near the head of the avalanche. The ions, both positive and negative, are scattered though out the plasma. The negative ion (O^-) density makes up from 30 to 40% of the total negative charge carriers. The average charge number density at the end of the forward discharge is about 10^{17} #/m³. Once the bulk of the electrons land on the dielectric (last frame of Fig. 5), very little further ionization is possible. The rest of the time, during the forward discharge, the ions recombine or move along the electric field imparting momentum to the neutrals. If they come in contact with the exposed electrode, they are also neutralized. The simulations show that the plasma eventually is extinguished in a time on the order of about 3 μ sec. This is much faster than the 200 μ sec period of the bias oscillation. The result is that the plasma is completely extinguished before the bias voltage reverses itself. This trait of the plasma actuator, that the plasma is created and extinguished during each *half* of the bias cycle, has also been observed in experiments.^{7,8}

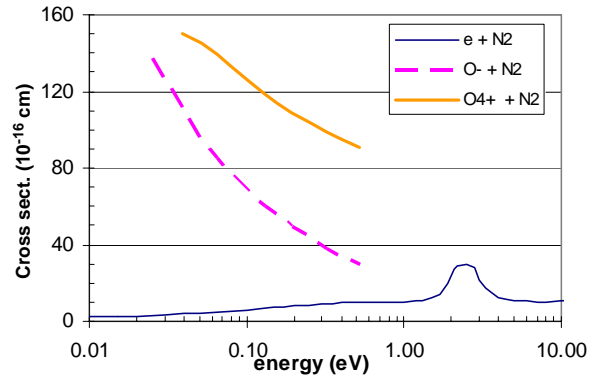


Figure 6. Momentum transfer cross section.

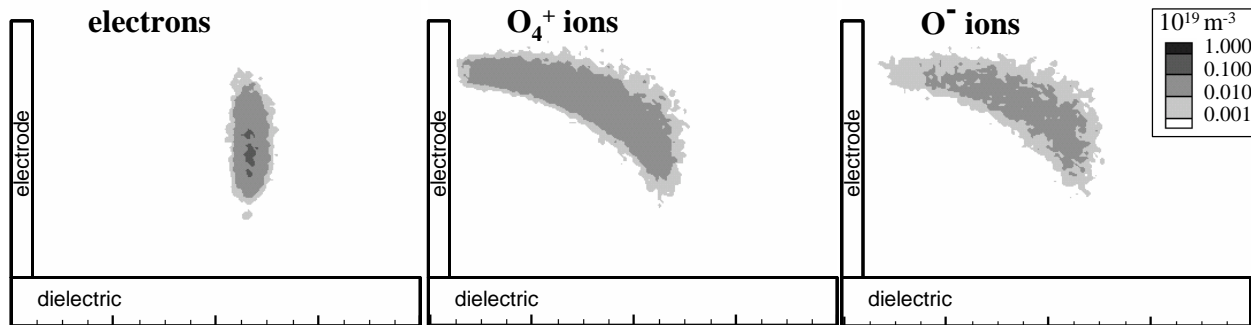


Figure 7. Charge number density 1 nsec into forward discharge.

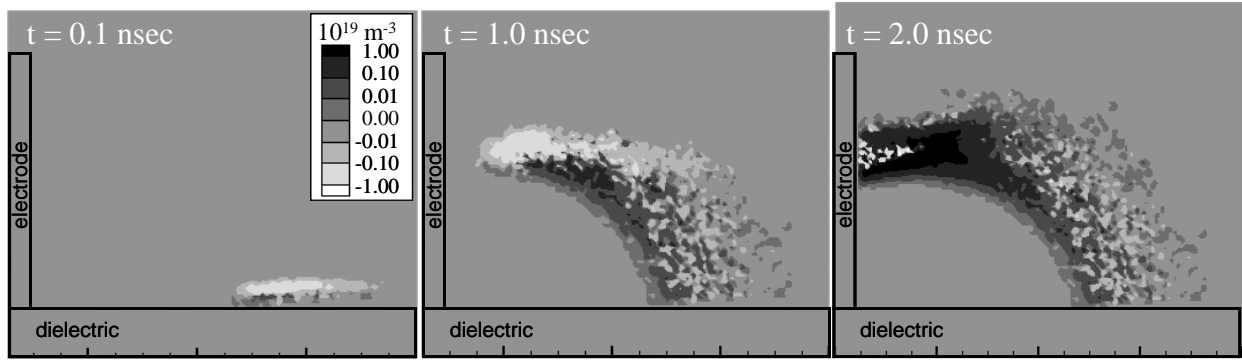


Figure 8. Charge number density during the beginning of the back discharge; Bias= 5200V.

At the end of the forward part of the discharge, only the negative charge carriers which impacted the dielectric before recombining remain. All other ions have been neutralized. The electrons are attracted to the dielectric by the imposed electric field but are kept from moving and gaining energy by the dielectric itself. When the bias field reverses during the second half of the bias cycle, however, the electrons are pushed away from the dielectric and are free to move. This is important because, although the forward discharge starts with a few thousand field effect or cosmic electrons, the back discharge (during the second half of the bias cycle) begins with hundreds of thousands or millions of electrons already present.

The first 2 nsec of the back discharge is shown in Fig. 8. The electrons are now attracted to the exposed electrode. As they accelerate and gain energy, they again undergo greater ionizing, dissociating, and meta-stable exciting collisions. Although, the electric field magnitude is not very different from that present during the forward discharge, a greater number of electrons are now available at the start. The result is a greater level of ionization. The individual electron, positive ion, and negative ion densities are shown in Fig. 9. The majority of the electrons are still concentrated near the head of the avalanche and the positive and negative ions are distributed throughout the avalanche. The average charge density is on the order of 10^{18} #/m^3 – ten times larger than during the forward discharge. The negative ions continue to be 30 to 40% of the negative charge carriers.

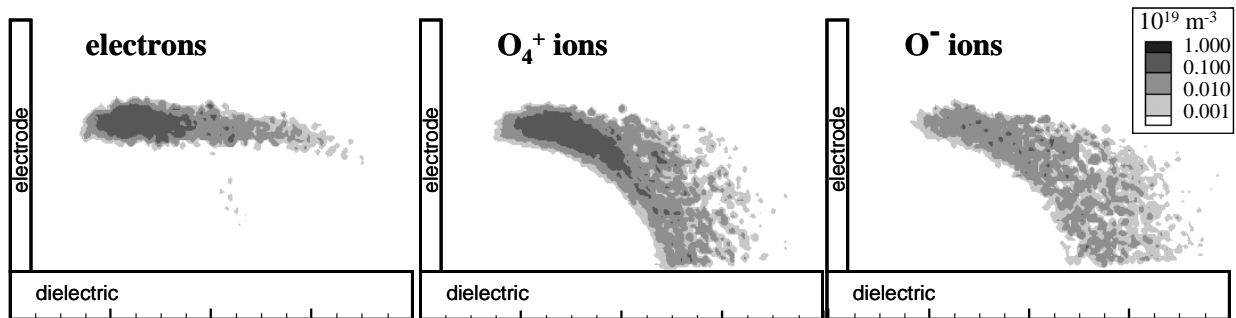


Figure 9. Charge number density 1 nsec into back discharge; Bias = 5200V .

The electrons which collide with neutrals do not only create ions, however, they also dissociate and excite the molecular oxygen. Fig. 10 displays the number density contours for the atomic oxygen and excited molecular oxygen. The atomic oxygen density peaks at $8 \times 10^{21} \text{ m}^{-3}$ while the excited molecular oxygen peaks at about $1 \times 10^{21} \text{ m}^{-3}$. Both are less than 1% of the ambient density and too small to contribute significantly to altering the chemical kinetics. However, this is after a single discharge cycle (forward and back). Since the neutral products of the discharge do not move significantly over many bias cycles, the products of subsequent bias cycles would probably accumulate and reach levels where the chemical kinetics, and, therefore, the discharge is affected. Excited and dissociated oxygen can provide additional paths toward ionization if their density levels become significant. Such accumulation of plasma products, however, was not modeled in this study and will be explored in the future.

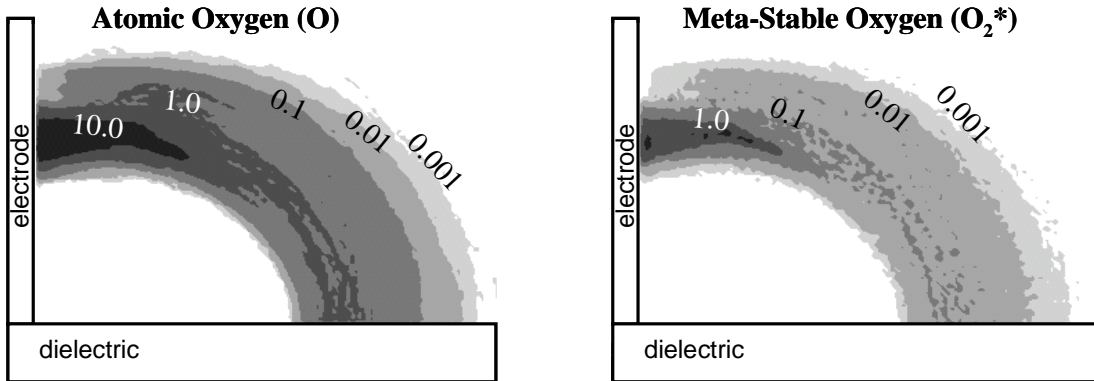


Figure 10. Atomic oxygen and excited molecular oxygen number density contours after a single (forward and back) discharge cycle (10^{20} m^{-3}).

B. Force Production

During the forward and back discharges, the electrons, positive ions, and negative ions undergo collisions with the neutral molecules. These collisions serve to transfer the momentum, which the ions and electrons gained from accelerating in the electric fields, to the neutral molecules. In the simulation, the momentum transfer from each collision which does not result in a chemical reaction is tabulated and stored. The resulting total momentum transfer vectors for the forward and back discharges are shown in Fig. 11. During the forward discharge, the electrons and negative ions are pushed away from the exposed electrode. Any collisions will, therefore, transfer momentum away from the exposed electrode. Conversely, the positive ions are pulled back toward the exposed electrode and transfer momentum back toward the electrode. The net momentum transfer is not zero, however, because of two reasons: 1) The electron momentum transfer collision cross section is much smaller than that of the ions, as shown in Fig. 6, resulting in a smaller number of collisions and diminished momentum transfer. And 2) the positive ions outnumber the negative ions by at least a factor of two. The result is that the net momentum transfer during the forward discharge from all of the charged species is toward the exposed electrode. This is a direction which is normally *against* the prevailing freestream flow. This result was unexpected when first noted in simulations of pure nitrogen¹¹ but was, in fact, later observed experimentally.¹²

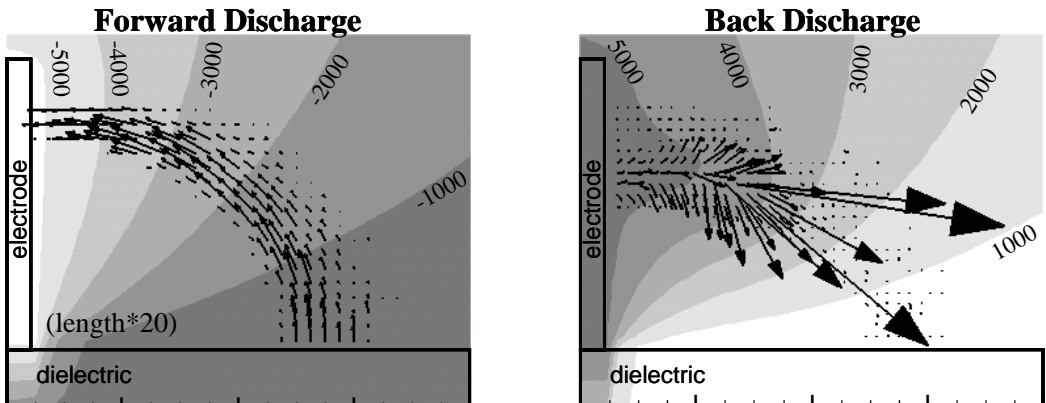


Figure 11. Total momentum addition vectors and potential contours (Volts) near the end of the forward and back discharges. The length of the vectors for the forward discharge are exaggerated for clarity.

During the back discharge, the external electric field and the momentum transfer reverse. The electrons and negative ions are pulled toward the exposed electrode and the positive ions are pushed away. As in the forward discharge, the momentum transfer from the positive ions is greater than from the negative ions and electrons. The resultant force for the back discharge is away from the exposed electrode and along the prevailing freestream direction. The momentum addition vectors for the back discharge are also shown in Fig. 11. The length of the

vectors is proportional to the force magnitude. The forward discharge vector lengths have been exaggerated by a factor of twenty for the purpose of clarity. Note that the force is not uniform in magnitude. Neither is it uniformly generated throughout the plasma.

A summation of the vector magnitudes reveals that the total force produced by the back discharge is greater than the total force produced by the forward discharge by at least a factor of ten. This is consistent with the observation that the average charge density during the back discharge is greater than during the forward discharge. The reason, therefore, that the plasma actuator net force is away from the exposed electrode appears to be due to the charge density being so much larger during the forward than during the back discharge. This trait does not appear to be altered by the presence of oxygen and is also found in the nitrogen discharges.

Comparing the initial potential contours (Fig. 4) with the contours at the end of the forward discharge (Fig. 11, forward discharge) reveals that the charge density is not sufficiently large to begin shielding the external field. Conversely, the potential contours at the end of the back discharge (Fig. 11, back discharge) are significantly altered, indicating that the plasma density during the back discharge reaches a level where shielding of the external field is possible.

This simulation was conducted for a single bias cycle. Since the plasma extinguishes during each half of the bias cycle, however, the results reported here are applicable to a continuously running plasma actuator. During each forward discharge the avalanche starts from a small number of electrons. It deposits most of the created electrons onto the dielectric, generates a force back toward the exposed electrode, and then extinguishes. During each back discharge, the avalanche begins from the large number of electrons created during the forward discharge which were deposited on the dielectric. It generates a net force away from the exposed electrode, and then extinguishes. The electrons generated during the back discharge either are neutralized on the exposed electrode or in recombination with the ions. Therefore, no significant amounts of charged species from the back discharge are present before the discharge begins in the forward direction once again. Consequently, the effects of each bias cycle are erased before the next bias cycle begins. The only important exception to this is, perhaps, the meta-stable and dissociated products, which may accumulate over many bias cycles.

C. Comparison with Experiments

One of the central questions in this study was whether the force production mechanism in air differed significantly from the mechanism in pure nitrogen. Pure oxygen, with its negative ions, represents one extreme in possible chemistry, while pure nitrogen, with only positive ions, represents the other extreme. Figure 12 shows the normalized time averaged force from the computations and the experiments.¹² The experiments were run in pure nitrogen and in air (21% O₂). The experimental results show that, when oxygen is present, the plasma flap produces more force. Further, the force produced in the presence of oxygen increases at a rate larger than pure nitrogen, as the voltage increases. The simulations do not reproduce the correct force magnitudes. They do, however, correctly predict higher force production in the presence of oxygen. They also correctly predict that the rate at which force increases with increasing voltage is higher in the presence of oxygen.

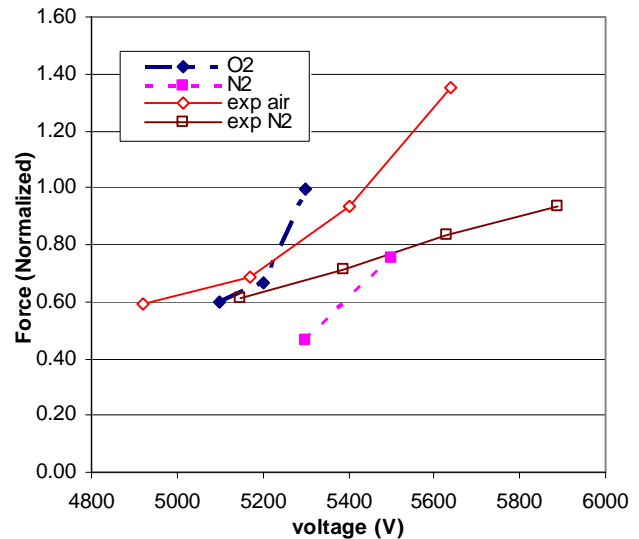


Figure 12. Normalized net force produced by the plasma actuator for the computation and experiments.

The simulations suggest that the presence of oxygen leads to greater force production because it results in greater levels of ionization. This is due to the oxygen ionizing at a lower energy than nitrogen. The presence of negative ions appears to mitigate this somewhat because the negative ions impart momentum to the air in a direction opposite to the positive ions. Since their density is not as large as that of the positive ions, however, they do not cancel the

force completely. Figure 13 shows the normalized force imparted during a complete bias cycle for a typical computational case. The force imparted by the positive ions is about a factor of 5 more than the force imparted by the negative ions and in the opposite direction. The electrons, due to their small momentum transfer collision cross section, impart only a small net negative force. Since the plasma must remain neutral, the limiting case where negative ions are as populous as positive ions would yield, at best, a net force of zero. The presence of negative ions, therefore, can never reverse the net force direction.

IV. Summary

Plasma actuators have demonstrated the ability to promote attachment of the flow around airfoils by providing momentum to the boundary layers. The method by which the momentum is imparted to the flow in air was the subject of the present study. A plasma actuator was simulated using PIC-DSMC methods at atmospheric pressure for pure nitrogen and a pure oxygen discharges. The electrodes were biased using a square wave function with a frequency of about 10 MHz. Both the electrons and ions were modeled as computational particles. The electric field was determined self-consistently during each time step. Collisions were resolved with the neutrals allowing for ionization, dissociation, dissociative attachment, meta-stable excitation, and momentum transfer.

The simulation results show that the plasma actuator imparts a force through collisional momentum transfer from the ions and electrons to the neutral molecules. The ions impart most of the momentum, when compared to the electrons, due to their larger momentum transfer cross section. During the first half of the bias cycle, the net force is back toward the exposed electrode. During the second half of the cycle, the force is away from the exposed electrode. The time averaged force from the plasma actuator is away from the exposed electrode because the force during the second half of the cycle is as much as ten times larger than during the first half. This is due to the charge density which can also be ten times larger during the second half of the bias cycle.

The presence of oxygen in the discharge results primarily in greater levels of ionization and the production of negative ions. The larger levels of ionization result in greater force production than in plasma discharges where no oxygen is present. The negative ions can number as much as 30 to 40% of the negative charge carriers in the plasma and effectively transfer momentum in a direction opposite to the positive ions. Because their density is smaller than the positive ions, however, the net force is not reversed when compared to a discharge, such as pure nitrogen, where all ions are positively charged.

Comparisons with experiments yield mixed results. Discharges containing oxygen are correctly predicted to generate larger forces. Discharges in pure nitrogen are correctly predicted to have a smaller increase in force from a fixed increase in bias voltage when compared to oxygen discharges. The force magnitudes, however, do not compare well with experiments. This may be due to dissociated and meta-stable plasma products which accumulate in the vicinity of the plasma actuator from one bias cycle to the next. These can result in altered ionization levels and different amounts of force production. This accumulation of plasma products was not modeled in the present study.

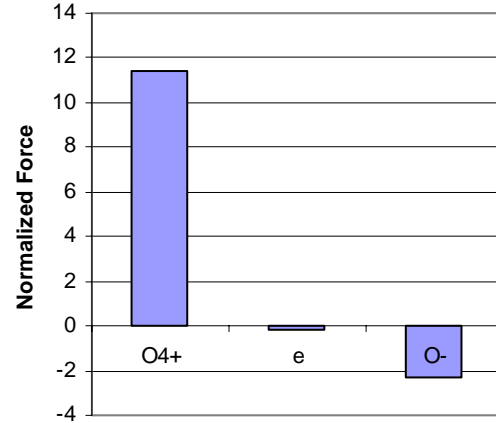


Figure 13. Normalized net force produced in a typical computational case during an entire bias cycle by positive ions, negative ions, and electrons.

References

- ¹Hultgren, L. S., and Ashpis, D. E., "Demonstration of Separation Delay with Glow-Discharge Plasma Actuators," AIAA Paper 2003-1025.
- ²List, J., Byerley, A. R., McLaughlin, T. E., and Van Dyken, R. D., "Using a Plasma Actuator to Control Laminar Separation on a Linear Cascade Turbine Blade," AIAA Paper 2003-1026.
- ³Roth, J. R., Sherman, D. M., and Wilkinson, S. P., "Boundary Layer Flow Control with a One Atmosphere Uniform Glow Discharge Surface Plasma," AIAA paper 98-0328.
- ⁴Post, M. and Corke, T., "Separation Control on High Angle of Attack Airfoil Using Plasma Actuators," *AIAA Journal*, Vol. 42, No. 11, 2004, pp. 2177.
- ⁵Huang, J., Corke, T. and Thomas, F., "Plasma Actuator for Separation Control of Low Pressure Turbine Blades," AIAA Paper 2003-1027.
- ⁶Rivir, R., White, A., Carter, C., Ganguly, B., Jacob, J., Forelines, A., and Crafton, J., "AC and Pulsed Plasma Flow Control," AIAA Paper 2004-0847.
- ⁷Enloe, C. L., McLaughlin, T. E., Van Dyken, R., Kachner, K. D., Jumper, E. J., Corke, T. C., Post, M., and Haddad, O., "Mechanisms and Responses of a Single Dielectric Barrier Plasma Actuator: Geometric Effects," *AIAA Journal*, Vol. 42, No. 3, 2004, pp. 595.
- ⁸Enloe, C. L., McLaughlin, T. E., Van Dyken, R., Kachner, K. D., Jumper, E. J., and Corke, T. C., "Mechanisms and Responses of a Single Dielectric Barrier Plasma Actuator: Plasma Morphology", *AIAA Journal*, Vol. 42, No. 3, 2004, pp. 589.
- ⁹Asghar, A., and Jumper, E. J., "Phase Synchronization of Vortex Shedding from Multiple Cylinders Using Plasma Actuators," AIAA Paper 2003-1028.
- ¹⁰Van Dyken, R., McLaughlin, T. E., and Enloe, C. L., "Parametric Investigations of a Single Dielectric Barrier Plasma Actuator," AIAA Paper 2004-0846.
- ¹¹Font, G. I., "Boundary Layer Control with Atmospheric Plasma Discharges," AIAA Paper 2004-3574.
- ¹²Enloe, C. L., McLaughlin, T. E., Font, G. I., and Baughn, J. W., "Parameterization of Temporal Structure in the Single Dielectric Barrier Aerodynamic Plasma Actuator", AIAA Paper 2005-0564.
- ¹³Birdsall, C. K., and Langdon, A. B., *Plasma Physics via Computer Simulation*, Adam Hilger, Bristol, 1991, Chap. 9.
- ¹⁴Font, G. I., and Boyd, I. D., "DSMC-PIC Simulation of a Helicon Etch Reactor and Comparison with Experiments," *Process Control, Diagnostics, and Modeling in Semiconductor Manufacturing*, Electrochemical Society, 1997, pp.275.
- ¹⁵VanGilder, D. B., Font, G. I., and Boyd, I. D., "Hybrid Monte Carlo Particle-in-Cell Simulation of an Ion Thruster Plume," *Journal of Propulsion and Power*, Vol. 15, No. 4, 1999, pp.530.
- ¹⁶Li, J., and Dhali, K., "Simulation of Microdischarges in a Dielectric-barrier Discharge", *J. Appl. Phys.*, Vol. 82, No. 9, 1997, pp. 4205.
- ¹⁷Kunhardt, E. E., and Tzeng, Y., "Development of an Electron Avalanche and its Transition into Streamers," *Phys Rev. A*, Vol. 38, No. 3, 1988, pp.1410.
- ¹⁸Phelps, A. V., and Pitchford, L. C., "Anisotropic Scattering of Electrons by N₂ and its Effects on Electron Transport: Tabulations of Cross Sections and Results," JILA Data Center Report No. 26, U. of Colorado, 1985.
- ¹⁹Pitchford, L. C., and Phelps, A. V., "Comparative Calculations of Electron-swarm Properties in N₂ at Moderate E/N Values," *Phys. Rev. A*, Vol. 25, 1982, pp.540.
- ²⁰Mitchell, J. B. A., "The Dissociative Recombination of Molecular Ions," *Physics Reports*, Vol. 186, 1990, pp.215.
- ²¹Ellis, H.W., Pai, R. Y., McDaniel, E. W., Manson, E. A., and Viehland, J. A., "Transport Properties of Gaseous Ions over a Wide Energy Range," *Atomic Data and Nuclear Data Tables*, Vol. 17, 1976, pp.177.
- ²²Phelps, A. V., "Tabulations of Collision Cross Sections and Calculated Transport and Reaction Coefficients for Electron Collisions with O₂," JILA Data Center Report No. 28, U. of Colorado, 1985.